RAA 2019 Vol. **19** No. **12**, 181(11pp) doi: 10.1088/1674–4527/19/12/181

http://www.raa-journal.org *http://iopscience.iop.org/raa*

Research in Astronomy and Astrophysics

Alignment between satellite and central galaxies in the EAGLE simulation: dependence on the large-scale environments

Ming-Ge Zhang and Yang Wang

School of Physics and Astronomy, Sun Yat-sen University, Zhuhai 519082, China; *wangyang23@mail.sysu.edu.cn*

Received 2019 April 19; accepted 2019 July 6

Abstract The alignment between satellite and central galaxies serves as a proxy for addressing the issue of galaxy formation and evolution, and has been investigated abundantly in observations and theoretical works. Most scenarios indicate that the satellites preferentially are located along the major axis of their central galaxy. Recent work shows that the strength of alignment signals depends on the large-scale environment in observations. We use the publicly-released data from EAGLE to figure out whether the same effect can be found in the associated hydrodynamic simulation. We found much stronger environmental dependency of alignment signals in the simulation. We also explore change of alignments to address the formation of this effect.

Key words: methods: statistical — methods: theoretical — galaxies: evolution — galaxies: general — cosmology: large-scale structure of Universe

1 INTRODUCTION

The standard Λ cold dark matter (ΛCDM) cosmology suggests a hierarchical scenario of cosmic structure formation. The growth of Gaussian density fluctuations via a highly nonlinear and anisotropic gravitational clustering process shapes the large scale structure of the Universe into four distinct environments, i.e., cluster, filament, sheet and void (Jõeveer et al. 1978; Bond et al. 1996). Flowing out of the voids, matter accretes onto the sheets, then collapses onto the filaments and finally assembles to form clusters at the intersections of filaments. On smaller scales, dark matter collapses to small halos firstly and then may go through mergers with other halos to form larger halos or be captured by larger halos to become their "subhalos," and galaxies are formed in the inner regions of these dark matter halos (White & Rees 1978). According to this paradigm, galaxies are not randomly distributed in the Universe, but rather show some alignments, i.e., the shape, position, spin, etc., which tend to have preferential directions (Jing & Suto 2002; Aubert et al. 2004; Bagla & Prasad 2006; Aragón-Calvo et al. 2010; Arieli et al. 2010). Thus, the galaxy alignment can be an indicator for probing galaxy formation and evolutionary history in the ΛCDM Universe.

Many observational and theoretical works have confirmed galaxy alignments. Explorations of galaxy alignments utilizing observation began with the early works (Sastry 1968 and Holmberg 1969). The former reported an alignment between satellite galaxies and major axis of central galaxies, but the latter claimed the opposite results that the position vectors of satellite galaxies tend to be perpendicular to the major axis of central galaxies. The disagreement between these two works may partly result from the small survey volume of the galaxy sample. Such a defect has been overcome by the emergence of large galaxy surveys, e.g., Sloan Digital Sky Survey (SDSS). Benefiting from a super-large volume of galaxy samples, studies on central-satellite galaxy alignments have already reached a unified and largely accepted conclusion that the satellites tend to align with the major axis of their central galaxy (e.g., Agustsson & Brainerd 2006b; Yang et al. 2006; Brainerd 2005; Agustsson & Brainerd 2010). Following theoretical works by utilizing semi-analytical models, both N-body simulations and hydrodynamical simulations have confirmed such a trend (Agustsson & Brainerd 2006a; Kang et al. 2007; Libeskind et al. 2005, 2007; Codis et al. 2012, 2015). For a full overview on all kinds of issues about galaxy alignments, in which the central-satellite alignment is just one aspect, readers can refer to Schäfer (2009), Joachimi et al. (2015), Kiessling et al. (2015) and Kirk et al. (2015).

The central-satellite alignment comes from the combination of smooth mass accretion and mergers of dark matter halos. The anisotropic collapse of a dark matter halo will shape its central galaxy with preferential directions (Jing & Suto 2002; Schäfer 2009). Consequently, the direction of axes, or angular momentum, of central galaxies will relate with their surrounding structures (Zhang et al. 2013, 2015). On the other hand, as remnants of accreted halos, merger events can be inferred from the positions of satellite galaxies. Therefore, the alignment between the positions of satellite galaxies and the directions of large scale structures was also studied (e.g., Tempel et al. 2015). However, detecting these two processes separately can be tough due to some ambiguities in defining the shape and direction of large scale structures from observational data, leading to most work focusing on the central-satellite alignments.

In the different structure types of the cosmic web, e.g., cluster, filament, sheet and void, the central-satellite alignment can be quite different, because of either dark matters collapsing via different directions (Codis et al. 2018), or subhalos (satellite galaxies) being accreted via different paths dictated by large scale structures (Libeskind et al. 2014). Accordingly, the shape of the central galaxy and the distribution of satellite galaxies may be influenced by the local structure types. Many works found that the shape of a dark matter halo, which should be aligned with its central galaxy, is related with local structures (Hahn et al. 2007; Zhang et al. 2009; Forero-Romero et al. 2014). Tempel & Libeskind (2013) concluded that the minor axes of elliptical galaxies are preferentially perpendicular to hosting filaments but the alignment signal is weak in sheets. Moreover, the spin axes of spirals align with host filaments, but there is no alignment signal between the spiral spin and the sheet normal vector. Codis et al. (2018) confirmed the same trend and further revealed an alignment flipping phenomenon from high to low redshifts. Some works like Tempel et al. (2015) confirmed that the angular positions of satellite galaxies tend to align with filaments. A further explanation is provided by Libeskind et al. (2015), in which they claimed that the plane of satellite galaxies' orbit is aligned well with the collapse direction derived from the shear tensor of environmental velocity fields.

Since the large scale structures influence both central galaxies and satellite galaxies, we would expect the alignment between them to depend on the local cosmic environments. It would be interesting to examine this issue, and recently Wang et al. (2018) engaged in such an exploration. Wang et al. (2018) found environmental dependence of the alignment between satellites and central galaxies in the SDSS Data Release 7 (DR7). Following Wang et al. (2018), we examine whether this dependence exists for simulated galaxies in cosmological hydrodynamical simulations, and investigate the possible explanation for this phenomenon.

This paper is organized as follows: we first briefly introduce the simulation, galaxy catalog definitions of large-scale structure and alignment angles in Section 2. Then the main results are given in Section 3. Finally, we provide discussions and conclusions in Section 4.

2 DATA AND METHODOLOGY

In this work, we use the publicly released data from the Evolution and Assembly of Galaxies and their Environments (EAGLE) simulation (Schaye et al. 2015), which was run using a modified version of the code GADGET-2 (Springel 2005). The cosmology parameters are $\Omega_m = 0.307$, $\Omega_b = 0.04825$, $\sigma_8 = 0.8288$, $n_s = 0.9611$ and $h = 0.6777$. We take advantage of the simulation run labeled "Ref-L100N1504", i.e., with a box size of $100\,\mathrm{Mpc}$, particle number of 2×1504^3 and softening length of $2.66\,\mathrm{kpc}$. The mass resolutions of gas and dark matter particles are $1.81 \times 10^6\,h^{-1}\,M_\odot$ and $9.70\times10^6\,h^{-1}\,M_\odot$ respectively. Stellar particles have variable mass around $7 \times 10^5\,h^{-1}\,M_\odot$. More details about the EAGLE simulation can be found in Schaye et al. (2015).

2.1 Galaxy Samples

We use five snapshots ($z = 0, 1, 2, 3, 5$) from the simulation for data analysis. The dark matter halos are identified by the standard friends-of-friends (FOF) algorithm (Davis et al. 1985). Dark matter particles within a linking length of 0.2 times the mean inter-particle separation are assigned to the same dark matter halo. Gas and star particles are assigned to the FoF halo in which their nearest dark matter particles reside. The subhalos are located by the SUBFIND algorithm (Springel et al. 2001; Dolag et al. 2009). We select central-satellite pairs from the $10\,000$ most massive dark matter halos. In remaining less massive halos, no satellite galaxies can be found due to the small number of star particles. We further constrain the galaxy sample such that only galaxies with more than 100 star particles are considered for analysis, corresponding to stellar mass of $7 \times 10^7\,h^{-1}\,M_\odot$. The number of central-satellite galaxy pairs selected is listed in Table 1.

Table 1 Number of Central-satellite Pairs Selected at Different Redshifts

z	0	1	2	3	5
Number of pairs	21 693	14 566	10 740	5914	1168

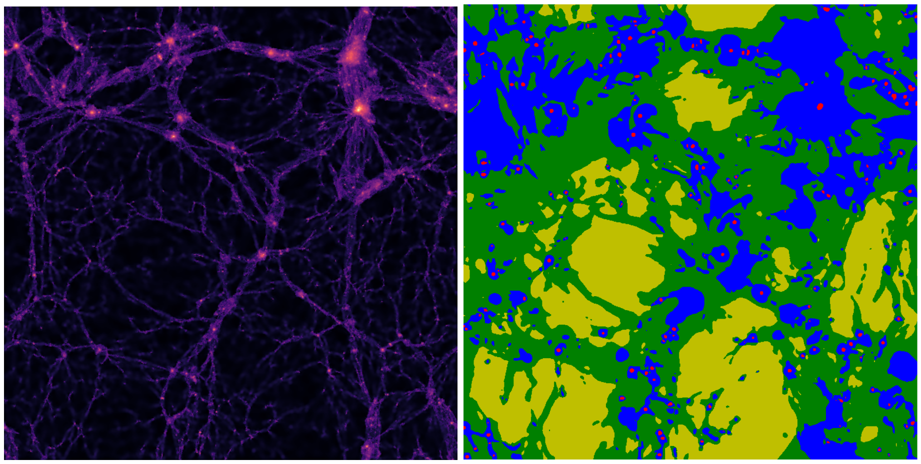

Fig. 1 Left panel displays the density field of a slice with volume of $100\,\mathrm{Mpc} \times 100\,\mathrm{Mpc} \times 60\,\mathrm{kpc}$ at redshift 0. Right panel indicates the large scale structure within the same region. *Red regions* are clusters, *green ones* are filaments, *blue ones* are sheets and *yellow ones* are voids.

2.2 Characterizing the Large Scale Environment

The structure types in the large scale environment, namely cluster, filament, sheet and void, are defined following the same method applied in Hahn et al. (2007), Forero-Romero et al. (2009) and Zhu & Feng (2017). We calculate the three eigenvalues of the Hessian matrix for the tidal field on specific grids

$$T_{i,j} = \frac{\partial^2 \phi}{\partial r_i \partial r_j}\,, \tag{1}$$

where ϕ is the potential there and i, j go from 1 to 3 to cover the three directions. For each grid, we count the numbers of eigenvalues above a certain threshold λ_t. If all three eigenvalues are larger than λ_t, the structure type around that point will be tagged cluster. Similarly, we sort out all particles, each with two, one or no eigenvalues larger than the threshold λ_t corresponding to filament, sheet and void respectively. In many works, λ_t is set to be 0 (Hahn et al. 2007). However, some works suggest a larger value of λ_t (Zhu & Feng 2017; Forero-Romero et al. 2009) to avoid producing a smaller volume of voids with $\lambda_t = 0$ than the theoretical prediction. Visually, a reasonable classification of the large scale structure can be given by setting $\lambda = 2.0$. Figure 1 displays the matter distribution (left) and corresponding environments (right) in a slice of simulation at redshift 0, where cells of different structures are assigned with different colors.

2.3 Characterizing the Alignment

In this paper, we analyze the alignment angle between the major axis direction of the central galaxy and the position direction of satellites, as illustrated in Figure 2. The yellow arrow represents the major axis of the central galaxy. The blue arrow signifies the direction of the satellite relative to the center of the central galaxy and θ_{CS} is the alignment angle. The major axis of the central galaxy is determined by the mass weighted shape matrix whose element is defined as

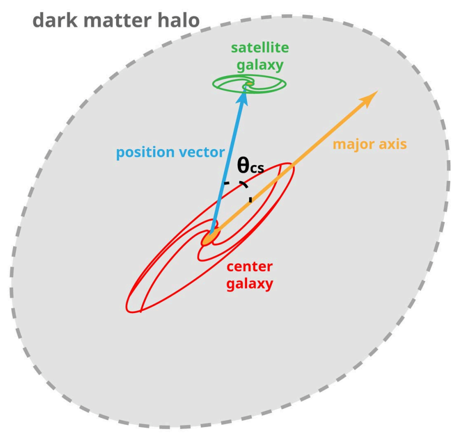

Fig. 2 A figure illustrating the central-satellite alignment angle. The *red* and *green ellipses* represent the central and satellite galaxies, respectively. The *yellow vector* signifies the major axis of the central galaxy. The *blue vector* is directed from the center of the central galaxy to the center of the satellite galaxy. The angular separation between *blue* and *yellow vectors* θ_{CS} is the alignment angle.

$$I_{ij} = \frac{\sum_k m_k x_{k,i} x_{k,j}}{\sum_k m_k}\,, \tag{2}$$

where m_k is the mass of the kth star particle in the central galaxy, $x_{k,i}$ is the coordinate of the kth star particle along the ith axis (i ranges from 1 to 3), and the summation is taken over all the star particles in the central galaxy. Once the shape matrix $I = \{I_{ij}, i, j = 1, 2, 3\}$ is obtained, the major axis can be specified by the eigenvector corresponding to the maximum eigenvalue of the shape matrix.

The alignment angle θ_{CS} ranges from 0° to 90°, and a relatively small value of $\theta < 45^\circ$ implies a preferen-

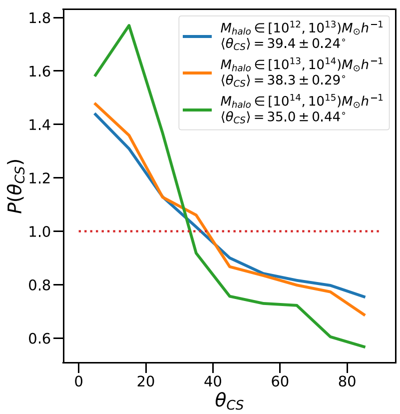

Fig. 3 The normalized probability distribution of the alignment angle θ_{CS}. Central-satellite pairs are assigned into three subsamples according to their host halo's mass, as indicated by the legend. The mean angle for each subsample is also expressed in the legend. The *red dotted horizontal line* $P = 1$ represents an ideal isotropic distribution.

tially aligned distribution along the major axis of the central galaxy. To compare with observations, we project the central galaxies and satellites onto a 2-dimensional (2-D) plane before calculating the alignment angle θ_{CS}. The projection onto the $x - y$ plane can be made simply by setting the z coordinate of all particles to be zero. We also tested projections onto the $x - z$ and $y - z$ planes. No significant differences have been found among the three projected directions. In the following, results are obtained by projecting galaxies onto the $x-y$ plane if not specified elsewhere.

3 RESULTS

In this section, we first present the color and mass dependence of central-satellite alignment following the previous works (Yang et al. 2006; Wang et al. 2018). Then we check numerically the dependence on various structure types in the cosmic web to test whether we could reproduce Wang et al. (2018)'s results. Finally, we make an attempt to explore the origin of dependency on large scale environment by tracing alignment signal θ_{CS} through cosmic time.

3.1 The Color and Mass Dependence of Central-satellite Alignments

Following Yang et al. (2006) and Wang & Kang (2018), we first check the overall alignment signal. As shown in the first row of Table 2, the mean alignment angle in the EAGLE simulation is smaller than those in Yang et al. (2006) and Wang & Kang (2018), indicating a stronger alignment. According to the previous works, e.g., Kang et al. (2007) and Faltenbacher et al. (2009), the alignment between subhalo and the major axis of the host halo is much stronger than that between satellite galaxies and the major axis of central galaxies. To reproduce the alignment signal inferred from the observations, the misalignment between central galaxy and host halo needs to be taken into account. Wang et al. (2014) and Faltenbacher et al. (2009) suggest a misalignment angle around 30°, which has been justified by Dong et al. (2014) using the hydrodynamical cosmological simulation. However, we calculate the misalignment between central galaxy and host halo in the EAGLE data, and found that it peaks at about 20°. This could be a reason why the stronger alignment signal has been found in that work. The physics behind such small misalignment might be complex, thus we leave it for future work.

Table 2 Mean alignment angle θ_{CS} for different (sub-)samples of central-satellite galaxy pairs at redshift 0 in the EAGLE simulation (fourth column), compared with the results in Yang et al. (2006) (second column) and Wang et al. (2018) (third column). Subsamples are divided according to galaxy color. In rows 2 to 3, only the color of central galaxies is considered. In rows 4 and 5, we only consider the satellites' color. In rows 6 to 9, the sample is constrained on both centrals and satellites. The sample name 'red - blue' means the galaxy pairs have red centrals and blue satellites.

Sample Name (1)	Y06 (2)	W18 (3)	This Work (4)
all samples	$42.2 \pm 0.2°$	$42.2 \pm 0.06°$	$38.1 \pm 0.3°$
red centrals	$41.5 \pm 0.2°$	$41.7 \pm 0.10°$	$38.2 \pm 0.3°$
blue centrals	$44.5 \pm 0.5°$	$44.7 \pm 0.15°$	$38.0 \pm 0.7°$
red satellites	$41.5 \pm 0.3°$	$41.5 \pm 0.11°$	$36.0 \pm 0.5°$
blue satellites	$43.3 \pm 0.3°$	$43.2 \pm 0.09°$	$39.3 \pm 0.3°$
red - red	$40.8 \pm 0.3°$	$40.9 \pm 0.12°$	$36.0 \pm 0.5°$
red - blue	$42.9 \pm 0.3°$	$42.6 \pm 0.13°$	$39.5 \pm 0.4°$
blue - red	$44.8 \pm 0.7°$	$45.5 \pm 0.31°$	$36.6 \pm 1.3°$
blue - blue	$44.2 \pm 0.6°$	$44.4 \pm 0.20°$	$38.4 \pm 0.8°$

The other rows in Table 2 list the color dependence of the alignment signal. The color of a galaxy is defined by its magnitude $g - r$. For the probability distribution of $g - r$, two peaks appear. We use the median value of these two peaks to classify galaxies into red and blue branches. This method was suggested by Baldry et al. (2004) and has been widely applied. In Yang et al. (2006) and Wang & Kang (2018), the red centrals or red satellites have smaller alignment angles. Galaxies in EAGLE are unable to fully reproduce such trends. In our samples, the red satellites align with the centrals' major axis more strongly, while the red and blue central galaxies have similar alignment signals. However, it is always a challenge to fully recover the alignment dependency on galaxy color. Our results are quite similar to those of Dong et al. (2014). Their results also eliminate the differences between blue and red central galaxies, which are basically caused by the fact that relatively more blue central galaxies are produced in the simulation than in observations. As displayed in figures 2

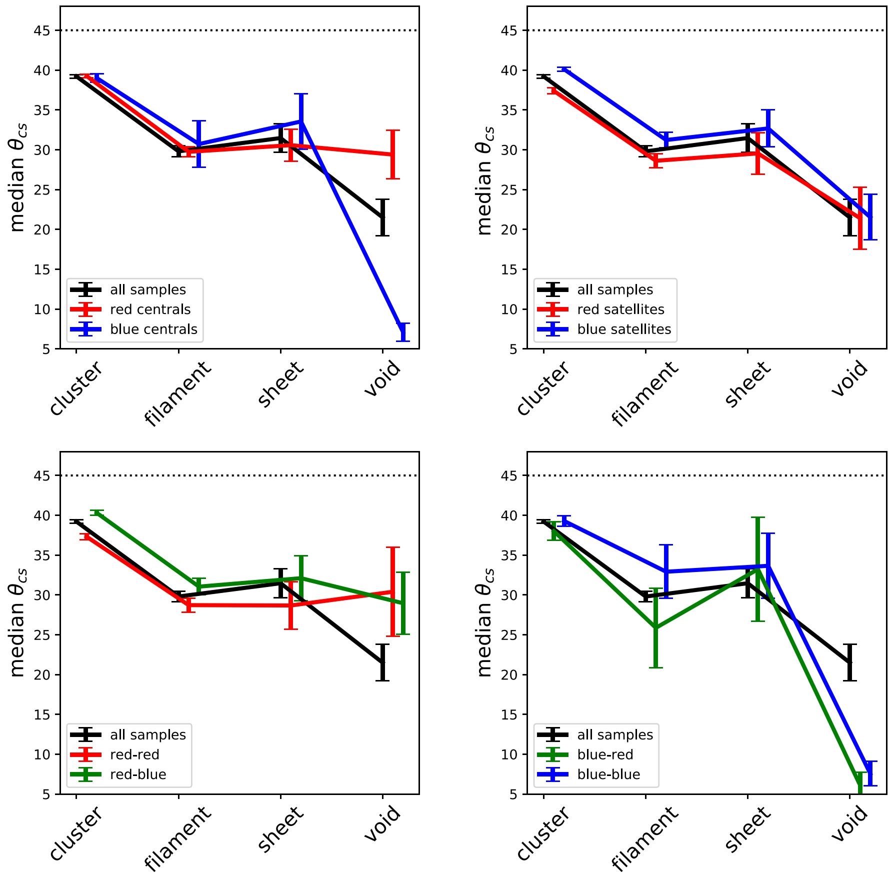

Fig. 4 Average alignment angle in different environments at redshift 0. Galaxy pairs are divided into different catalogs according to the color of central or satellite galaxies. The *upper-left panel* illustrates the difference between galaxy pairs with red and blue centrals. The upper-right panel compares the samples with red satellites and blue satellites. The *lower-left panel* displays red centrals - red satellites samples versus red centrals - blue satellites, while the *lower right* one shows blue centrals - red satellites sample versus blue centrals - blue satellites sample. A *black solid line* indicating the overall trend is drawn in all panels. The *black dotted line* at $\langle\theta\rangle = 45°$ represents the average alignment level of the random distribution of satellites. The error bars indicate the Poisson error of mean θ_{CS}. To make the error bars clear, we slightly shift lines horizontally.

and 4 in Trayford et al. (2015), the $g - r$ versus M_* or $g - r$ versus M_r profile in the EAGLE simulation has similar outer shape and blue peak as GAMA galaxies, but it does not recover the red peak. Thus some central galaxies with strong alignment are mis-assigned to blue color. Trayford et al. (2015) suggested that the flat slope of the red sequence may be attributed to the rapidly decreasing stellar metallicity at the low mass range, and such decrement may be a resolution issue in the simulation.

We also check the dependence on mass of the host halo. The probability distribution of the alignment angle θ_{CS} is shown in Figure 3. The probability distribution is obtained by computing $P(\theta) = N(\theta)/N_R(\theta)$. $N(\theta)$ is the number of central-satellite pairs with the alignment angle of θ in the samples to be studied. $N_R(\theta)$ is the number of galaxy pairs with the same θ in a sample with randomly distributed satellite galaxies. The total number of galaxy pairs in a random sample is the same as that in the simulation sample. Figure 3 demonstrates that the alignment is clearly dependent on the halo mass. Galaxy pairs in the massive halos exhibit stronger alignment. These trends are in agreement with Yang et al. (2006), Kang et al. (2007), Wang et al. (2014) and Wang & Kang (2018).

In summary, the EAGLE's galaxy catalog reproduces both the mass and color dependence (partly) of alignment in the observations. It also encounters problems such as too strong an alignment signal and blue biased central galaxies, but these problems also exist in many other simulations. On the other hand, the overall trend is quite reasonable. Thus the drawback does not affect the main part of our work, exploring the environmental effect of large scale structures on the alignment.

3.2 The Environment Influence of Large Scale Structures

To explore the dependence of central-satellite alignment angle on the large-scale environment, we first calculate the

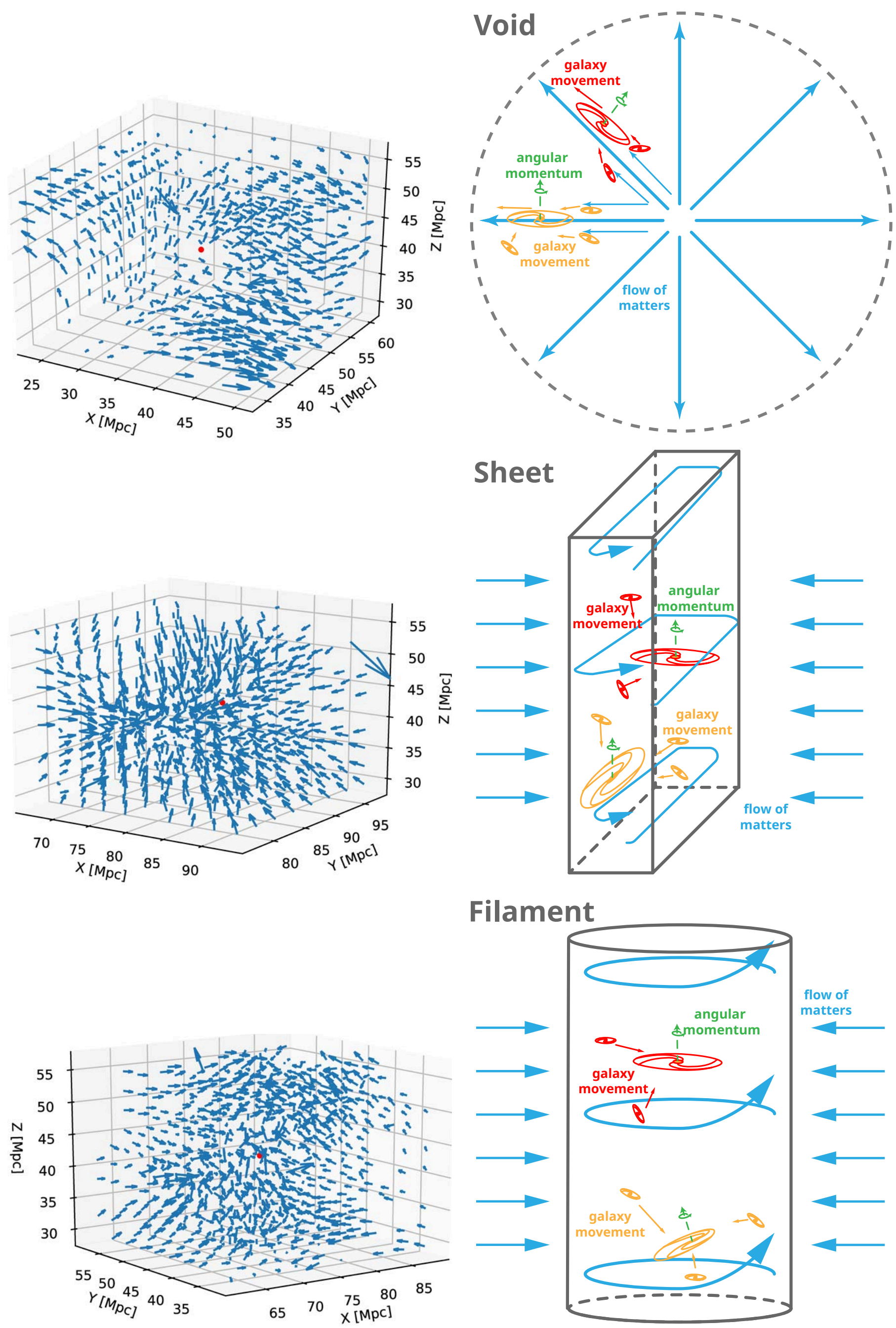

Fig. 5 The *left column* shows the velocity field of a $10\,\mathrm{Mpc}^3$ box around the center of void, sheet and filament. In the *right column*, we use diagrams to illustrate the movement of galaxies (*red* and *yellow arrows*) and matters in the background (*blue arrows*), as well as the possible alignment patterns between central and satellite galaxies. From *top to bottom*, each row depicts the situation of one environment, i.e., void, sheet and filament. The velocity field of clusters is very messy, thus we do not include its figures here.

median angles in the cases cluster, filament, sheet and void, which are depicted in Figure 4. The exact values of mean angle are provided in Table 3.

As is apparent in Figure 4, the alignment signals are increasing from environments of cluster to filament, sheet then void. This trend is much stronger than the results in Wang et al. (2018). Such environmental dependency can be explained by tracing the accretion history in the different large-scale environments (Codis et al. 2012). To illustrate this, we plot Figure 5.

In void, the matter flows radially away from the central region to the surrounding dense region. The velocity field of void in the top-left subplot of Figure 5 manifests this trend clearly. During this process, the angular momen-

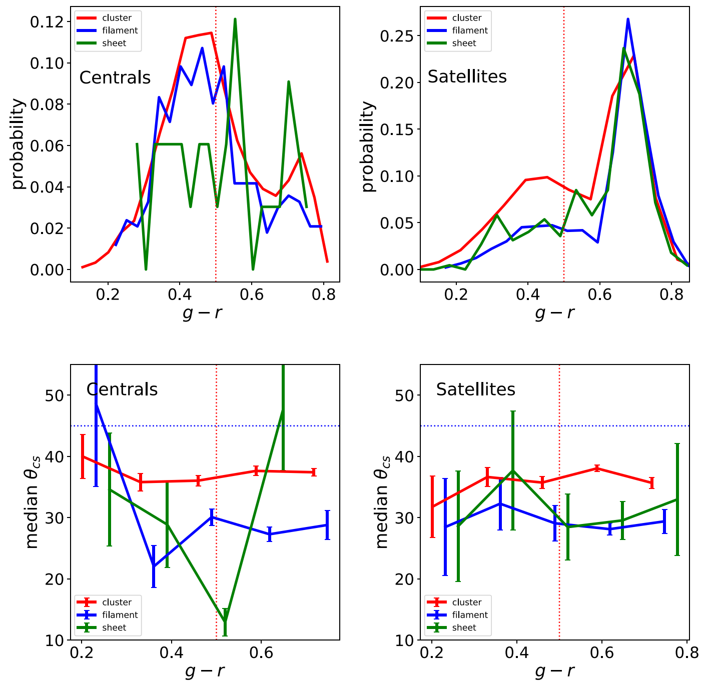

Fig. 6 The *upper two panels* plot the distribution of central galaxies' color (*upper left*) and satellite galaxies' color (*upper right*). *Lower panels* depict the mean alignment angle θ_{CS} as a function of central galaxies' color (*lower left*) and satellite galaxies' color (*lower right*). Curves for different subsamples are distinguished by color as the legend shows. *Red dotted vertical lines* mark the division between blue and red galaxies. In the *lower panels*, the *black dotted horizontal lines* signify the average alignment angle of a random distribution. We do not include void galaxies here because there are too few of them. To make the error bars clear, we slightly shift lines horizontally.

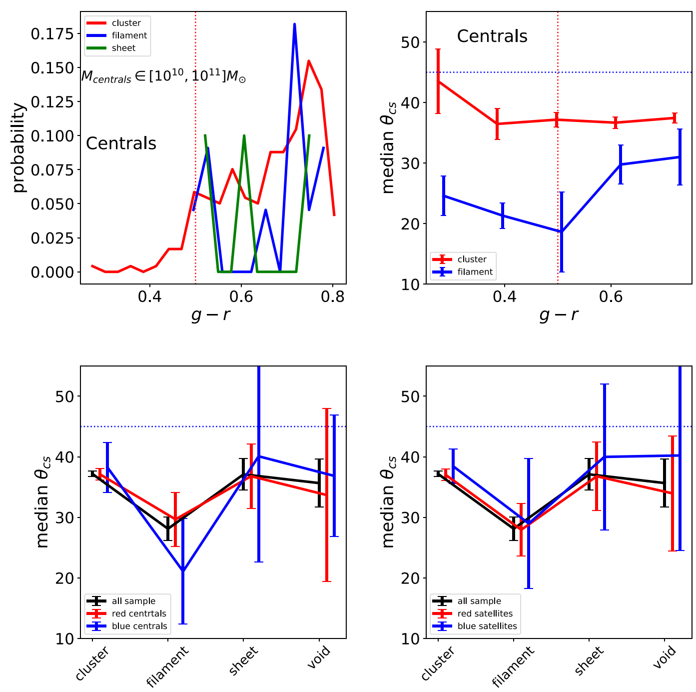

Fig. 7 *Top-left* subplot displays the color distribution of central galaxies with mass of $10^{10} \sim 10^{11}\ M_\odot$. The pattern is the same as the *top-left* subplot of Fig. 6. Other subplots show the alignment of galaxy pairs with central galaxies within the same range. The *top right* subplot illustrates the relation between median alignment angle and color of central galaxies, which is the same as that in the *bottom-left* subplot in Fig. 6. The curves for sheet and void galaxies are not included because there are few samples. *Two bottom* subplots depict the alignment-environment relations for galaxies with different colors, which are the same as in the top rows of Fig. 4.

Table 3 The mean θ_{CS} in different environments. Subsamples are the same as in Table 2. For short, "satellite galaxy" is written as "sat".

	Cluster	Filament	Sheet	Void
all samples	$39.2 \pm 0.2°$	$29.8 \pm 0.7°$	$31.5 \pm 1.7°$	$21.5 \pm 2.2°$
red central	$39.3 \pm 0.3°$	$29.7 \pm 0.7°$	$30.6 \pm 2.0°$	$29.4 \pm 3.0°$
blue central	$39.0 \pm 0.6°$	$30.7 \pm 2.8°$	$33.5 \pm 1.2°$	$7.1 \pm 1.2°$
red sat	$37.4 \pm 0.4°$	$28.6 \pm 0.9°$	$29.5 \pm 2.7°$	$21.4 \pm 4.0°$
blue sat	$40.1 \pm 0.3°$	$31.2 \pm 1.0°$	$32.7 \pm 2.3°$	$21.5 \pm 2.8°$
red - red	$37.3 \pm 0.4°$	$28.7 \pm 0.8°$	$28.7 \pm 2.8°$	$30.4 \pm 5.3°$
red - blue	$40.3 \pm 0.3°$	$31.0 \pm 1.0°$	$32.1 \pm 2.7°$	$28.9 \pm 3.9°$
blue - red	$38.0 \pm 1.2°$	$25.8 \pm 4.7°$	$33.2 \pm 6.6°$	$6.1 \pm 1.6°$
blue - blue	$39.3 \pm 0.6°$	$32.9 \pm 3.5°$	$33.6 \pm 4.0°$	$7.5 \pm 1.5°$

tum of the gas is thus perpendicular to the radial direction, leading to the axis of the galaxy formed more likely aligning with the same radial direction, as represented by the top-right subplot of Figure 5. On the other hand, the galaxies that formed in voids always tend to move outward radially, on which the satellite accretions occur. By this way, the alignment of the satellite galaxies is likely to be along the main axis of the central galaxy, producing the stronger alignment signals. Trujillo et al. (2006), Brunino et al. (2007) and Varela et al. (2012) found that galaxies at the edge of void have a rotation axis both parallel to the outer boundary of void and perpendicular to the radial direction, which is in agreement with our conclusion.

According to Zeldovich's approximation, the gas accretion is always anisotropic and the sheets usually appear firstly during the formation of cosmic web, because there is always one direction along which the matter collapse is fastest, corresponding to the maximum eigenvalue of the deformation matrix, so as to first form a 2-D pancake, i.e., the sheet structure. While being accreted onto sheets from both sides, the gas almost keeps its angular momentum parallel to the plane of sheets. Consequently, the galaxies that formed on the sheet have their angular momentum parallel to the sheet plane, as the middle-right subplot of Figure 5 shows. Meanwhile, the major axis could be either perpendicular (red central galaxy, middle-right subplot of Fig. 5) or parallel (orange central galaxy) to the sheet, or else lying in an intermediate state between them. However, for the satellite galaxies, the accretion occurs in the sheet plane where the galaxies are assembled. Therefore, it is possible that the position vectors of the satellite galaxies are perpendicular to the major axes of the central galaxy, causing the alignment signals to weaken and θ_{cs} to increase.

Matter in sheets would collapse further and form filaments. Gas swirls around and flows into filaments to form spirals that have angular momentum aligned along the direction of filaments, as bottom subplots in Figure 5 illustrate. Therefore, newly formed galaxies (usually blue disk galaxies) tend to have their major axis perpendicular to filaments (Codis et al. 2015; Welker et al. 2018). Since galaxies form within the cylinder of a filament, they gather together via the direction of the filament. We check the entering direction of satellites in filaments. In our samples, 60.7% of satellites have theirangles between their position vectors at entering time and the direction of filaments is smaller than $60°$. Note that $60°$ is the mean value of angular separation for satellites with random distribution in 3-D space. Thus, satellites enter their host halo in a direction that is perpendicular to the plane of the central galaxy. The alignment signal becomes weaker. However, since the shape of central galaxies changes as they also keep accreting gas from filaments, their major axis will be gradually redirected to the direction of filaments. On the other hand, early accreted satellite galaxies will move closer to the major axis of central galaxies when they fall closer to them. Because of these two mechanisms, old red central galaxies consequently present stronger alignment signals (Yang et al. 2006; Welker et al. 2018).

In clusters, satellite galaxies are more likely to come from the conjunction of filaments. However, for an individual galaxy, surrounding gas is so diffuse with complex movement that it can be accreted in any direction. Early formed central galaxies may have their satellites and accreted mass via the same direction, because at the early stage of cluster growth, gas may flow in the same direction as satellites. For those late formed galaxies, the position of accreted satellite could be totally irrelevant to incoming gas.

The above descriptions are favored by many works (e.g., Codis et al. 2012, 2015; Welker et al. 2018). They can explain well the influence of large scale structures on galaxies' central-satellite alignments. However, the alignment signal in simulation is much stronger than that in observations, which indicates that the simulations might have not fully reconstructed the nonlinear process and sub-grid physics such as thermal and kinetic feedback.

When we examine galaxy color, we found that the dependency on large scale environments is not influenced by the color of centrals or satellites. The curves of subsamples have nearly the same slope as the black curve of the whole sample, while the amplitude shift stays almost constant in all environments. Only in voids does the θ_{CS} of blue centrals fall rapidly while that of red centrals becomes flat. This sudden change may not be reliable, since the number of galaxy pairs in voids is much less than in other environments.

Most parts of these θ_{CS}-environment curves have the same trends as Wang et al. (2018)'s work. In their results, the alignment of blue centrals is strongly dependent on environment, but that of red centrals is not. For the EAGLE galaxies, blue and red centrals have the same θ_{CS} in clusters, but SDSS DR7 data manifest significant discrepancy between red and blue centrals in clusters.

We also investigated the color dependence on the environments. We found a blue biased central galaxy group, as Figure 6 illustrates. The galaxy color distribution is almost the same in cluster, filament and sheet, except that satellites in clusters have an extra peak in the blue region. This distribution is totally different from that exhibited by SDSS data (Wang et al. 2018). In Wang et al. (2018), the probability distribution of central galaxies has its peak at the red part, and the fraction of blue galaxies increases from clusters to sheets. In the lower panels, we found that θ_{CS} is independent of $g-r$ in clusters. In filaments, θ_{CS} decreases slightly with galaxy color. The relation becomes unstable in sheets due to the limited galaxy number. In Wang & Kang (2018), the alignment-color relation has a steadily falling trend in all environments, and the slopes are identically the same.

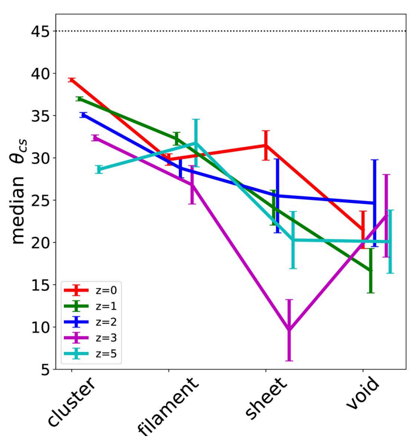

Fig. 8 Alignment angle distribution in different environments at different redshifts. Alignment-environment relation curves for different redshifts are distinguished by different colors as the legend shows. The *black dashed line* at θ_{CS} indicates the alignment angle of a random distribution. To make the error bars clear, we slightly shift lines horizontally.

We have found that EAGLE galaxies do not fully recover the same color distribution as observations. However, we cannot say that this is the only reason for the inconsistency in the color dependence of alignment-environment relation between this work and Wang et al. (2018). Guo et al. (2016) claimed that, in the EAGLE simulation, the passive fraction of galaxies with mass between 10^{10} and $10^{11}\,M_\odot$ is quite reasonable compared with observations. Thus, we further check the alignment of galaxy pairs with central galaxies within this range. The top-left subplot of Figure 7 demonstrates that, for a specific central galaxy mass range, the color distribution is much closer to observations (see fig. 3 in Wang et al. (2018)). However, the top-right subplot tells us the θ_{cs} - $(g-r)$ relation of this

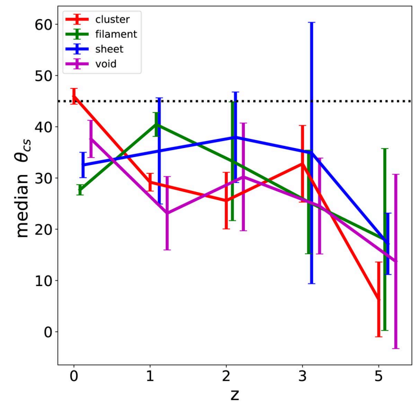

Fig. 9 The change of mean alignment angle for galaxies in four dark matter halos. Four halos are selected from different large scale structures, i.e., cluster, filament, sheet and void. Each line represents the statistic of galaxy alignment between one central galaxy and its satellite galaxies. To make the error bars clear, we slightly shift lines horizontally.

subsample is still inconsistent with Wang et al. (2018)'s results. Moreover, the alignment angle is less related with environment for both blue and red galaxies, while in observations blue centrals have a stronger alignment signal than red centrals (Wang et al. 2018). Such differences imply that, even for a galaxy catalog with the correct color distribution, the alignment - color relation is not recovered well due to some sophisticated sub-grid physics.

3.3 Alignment at High Redshift

In order to investigate the evolution of the alignment angle, we also calculate the alignment angle at higher redshifts, e.g., $z = 1, 2, 3, 5$, Figure 8 illustrates the probability distribution of the alignment angle at those redshifts. We found that the alignment-environment correlation exists at all redshifts. The strength of the alignment signal increases from clusters, filaments to sheets then voids. The slopes of those curves at different redshifts are quite close, implying that the difference between structures does not change significantly for a long time. As we have mentioned in Section 3.2, the alignment comes from the different mass accretion paths of both central and satellite galaxies. A reasonable scenario is that the mass accretion follows different paths in the different large scale environments, resulting in the environmental dependency of the alignment. Thus, we expect environmental dependency of alignment whenever large scale structures exist.

In clusters, central-satellite galaxy pairs exhibit stronger alignment signals at higher redshifts. This evolution trend still exists in filaments, but merely becomes observable in sheets and voids. It is found that early accreted satellites, in other words satellites closer to the central galaxies, prefer to align along the galaxies' major axis

(Yang et al. 2006; Faltenbacher et al. 2008; Wang & Kang 2018). One possible explanation is that the satellites move closer to the major axis after falling into their host halo (Welker et al. 2018). However, our Figure 8 implies another possible routine: early accreted satellites tend to enter their host halos in paths that are closer to the major axis than those entering late. Late accreted satellites dilute their alignment signal, resulting in increasing average θ_{CS}.

To confirm which process dominates the evolution of central-satellite alignments, we choose four central galaxies to trace how the alignment angles of their satellites evolve with redshifts. These four central galaxies are deliberately chosen from the four different structure types. For each central galaxy, we calculate the mean θ_{CS} of its satellites at each snapshot, then plot $\langle\theta_{CS}\rangle$ versus z in Figure 9. In Figure 9, $\langle\theta_{CS}\rangle$ of cluster galaxies decreases from $z = 0$ to $z = 5$. This supports our previous assumption that the early accreted satellites were accreted closer to the major axis of the central galaxy than the late accreted ones. The filament, sheet and void galaxies do not have monotonically changing evolution curves. That is why we did not observe alignment angle weakening with time in other structures except clusters.

4 CONCLUSIONS AND DISCUSSION

Using data from the EAGLE hydrodynamic simulation, we explore the large-scale environment dependence of the alignment angle between the central galaxy major axis and the satellite galaxy position vector. This is mainly a follow up work of Wang et al. (2018), thus all results are compared with their results based on SDSS observation data. The general conclusions are summarized below:

- Inconsistent with the results in Wang et al. (2018), the alignment signal between the major axis of central galaxies and the position vector of satellite galaxies in EAGLE simulations exhibits environmental dependence. Average alignment angle decreases gradually when the environment changes from cluster to filament, sheet and void. However, the amplitude of alignment signal in simulation and the environmental dependency are much stronger than the results extracted from observations. Further improvements on the subphysics of simulation may overcome this discrepancy. It is also possible that observational contamination dilutes the alignment signal.
- We found that EAGLE galaxies do not recover the dependency of alignment on galaxy color. The fact that EAGLE produces more blue central galaxies than observations accounts for emergence of this bias. However, the trends are not right even for subsamples with correct color distribution. It is possible that the colors of both red and blue galaxies are wrongly assigned. To verify this, a through investigation into subgrid physics is required in future works.
- We found that the influence of large scale structures exists at high redshifts. It demonstrates that the phenomenon of alignments of satellite galaxies is mainly a dynamically driven process, which is largely determined by the flows of matters.

Comparing with the alignment signal extracted from observations in Wang et al. (2018), there are two main differences in our results: the alignment signal is too strong and galaxy colors are mis-assigned. However, it is still worthwhile to consider the large scale structure effect on alignment within the scope of simulations. The simulations basically reproduce the trends for overall alignment signal and for the dependency on large scale environments. Since the dynamic processes of simulations are promising, we can explore the factors driving large scale structure dependency. We confirm that the alignment signal reported in this work and that in Wang et al. (2018) can be explained by the matter accretion scenario proposed in previous works (Codis et al. 2015, 2012; Welker et al. 2018).

Acknowledgements We thank the referee for through comments and suggestions to this paper. YW is supported by NSFC (No. 11803095), and YW and ZMG are supported by NSFC (No. 11733010). ZMG thanks Weishan Zhu for helpful discussions and suggestions. We acknowledge the Virgo Consortium for making their simulation data available. The EAGLE simulations were performed using the DiRAC-2 facility at Durham, managed by the ICC, and the PRACE facility Curie based in France at TGCC, CEA de Bruyères-le-châtel.

References

Agustsson, I., & Brainerd, T. G. 2006a, ApJ, 650, 550
Agustsson, I., & Brainerd, T. G. 2006b, ApJ, 644, L25
Agustsson, I., & Brainerd, T. G. 2010, ApJ, 709, 1321
Aragón-Calvo, M. A., van de Weygaert, R., & Jones, B. J. T. 2010, MNRAS, 408, 2163
Arieli, Y., Rephaeli, Y., & Norman, M. L. 2010, ApJ, 716, 918
Aubert, D., Pichon, C., & Colombi, S. 2004, MNRAS, 352, 376
Bagla, J. S., & Prasad, J. 2006, MNRAS, 370, 993
Baldry, I. K., Balogh, M. L., Bower, R., Glazebrook, K., & Nichol, R. C. 2004, in American Institute of Physics Conference Series, 743, The New Cosmology: Conference on Strings and Cosmology, eds. R. E. Allen, D. V. Nanopoulos, & C. N. Pope, 106
Bond, J. R., Kofman, L., & Pogosyan, D. 1996, Nature, 380, 603
Brainerd, T. G. 2005, ApJ, 628, L101
Brunino, R., Trujillo, I., Pearce, F. R., & Thomas, P. A. 2007, MNRAS, 375, 184

Codis, S., Jindal, A., Chisari, N. E., et al. 2018, MNRAS, 481, 4753
Codis, S., Pichon, C., Devriendt, J., et al. 2012, MNRAS, 427, 3320
Codis, S., Pichon, C., & Pogosyan, D. 2015, MNRAS, 452, 3369
Davis, M., Efstathiou, G., Frenk, C. S., & White, S. D. M. 1985, ApJ, 292, 371
Dolag, K., Borgani, S., Murante, G., & Springel, V. 2009, MNRAS, 399, 497
Dong, X. C., Lin, W. P., Kang, X., et al. 2014, ApJ, 791, L33
Faltenbacher, A., Jing, Y. P., Li, C., et al. 2008, ApJ, 675, 146
Faltenbacher, A., Li, C., White, S. D. M., et al. 2009, RAA (Research in Astronomy and Astrophysics), 9, 41
Forero-Romero, J. E., Contreras, S., & Padilla, N. 2014, MNRAS, 443, 1090
Forero-Romero, J. E., Hoffman, Y., Gottlöber, S., Klypin, A., & Yepes, G. 2009, MNRAS, 396, 1815
Guo, Q., Gonzalez-Perez, V., Guo, Q., et al. 2016, MNRAS, 461, 3457
Hahn, O., Porciani, C., Carollo, C. M., & Dekel, A. 2007, MNRAS, 375, 489
Holmberg, E. 1969, Arkiv for Astronomi, 5, 305
Jõeveer, M., Einasto, J., & Tago, E. 1978, MNRAS, 185, 357
Jing, Y. P., & Suto, Y. 2002, ApJ, 574, 538
Joachimi, B., Cacciato, M., Kitching, T. D., et al. 2015, Space Sci. Rev., 193, 1
Kang, X., van den Bosch, F. C., Yang, X., et al. 2007, MNRAS, 378, 1531
Kiessling, A., Cacciato, M., Joachimi, B., et al. 2015, Space Sci. Rev., 193, 67
Kirk, D., Brown, M. L., Hoekstra, H., et al. 2015, Space Sci. Rev., 193, 139
Libeskind, N. I., Cole, S., Frenk, C. S., Okamoto, T., & Jenkins, A. 2007, MNRAS, 374, 16
Libeskind, N. I., Frenk, C. S., Cole, S., et al. 2005, MNRAS, 363, 146
Libeskind, N. I., Hoffman, Y., Tully, R. B., et al. 2015, MNRAS, 452, 1052
Libeskind, N. I., Knebe, A., Hoffman, Y., & Gottlöber, S. 2014, MNRAS, 443, 1274
Sastry, G. N. 1968, PASP, 80, 252
Schäfer, B. M. 2009, International Journal of Modern Physics D, 18, 173
Schaye, J., Crain, R. A., Bower, R. G., et al. 2015, MNRAS, 446, 521
Springel, V., White, S. D. M., Tormen, G., & Kauffmann, G. 2001, MNRAS, 328, 726
Springel, V. 2005, MNRAS, 364, 1105
Tempel, E., Guo, Q., Kipper, R., & Libeskind, N. I. 2015, MNRAS, 450, 2727
Tempel, E., & Libeskind, N. I. 2013, ApJ, 775, L42
Trayford, J. W., Theuns, T., Bower, R. G., et al. 2015, MNRAS, 452, 2879
Trujillo, I., Carretero, C., & Patiri, S. G. 2006, ApJ, 640, L111
Varela, J., Betancort-Rijo, J., Trujillo, I., & Ricciardelli, E. 2012, ApJ, 744, 82
Wang, P., & Kang, X. 2018, MNRAS, 473, 1562
Wang, P., Luo, Y., Kang, X., et al. 2018, ApJ, 859, 115
Wang, Y. O., Lin, W. P., Kang, X., et al. 2014, ApJ, 786, 8
Welker, C., Dubois, Y., Pichon, C., Devriendt, J., & Chisari, N. E. 2018, A&A, 613, A4
White, S. D. M., & Rees, M. J. 1978, MNRAS, 183, 341
Yang, X., van den Bosch, F. C., Mo, H. J., et al. 2006, MNRAS, 369, 1293
Zhang, Y., Yang, X., Faltenbacher, A., et al. 2009, ApJ, 706, 747
Zhang, Y., Yang, X., Wang, H., et al. 2013, ApJ, 779, 160
Zhang, Y., Yang, X., Wang, H., et al. 2015, ApJ, 798, 17
Zhu, W., & Feng, L.-L. 2017, ApJ, 838, 21